

Reversibly thermochromic and high strength core-shell nanofibers fabricated by melt coaxial electrospinning

Shuoshuo Wang¹ | Liqiang Yi¹ | Yini Fang¹ | Lina Wang¹ | Juming Yao¹ | Jaromir Marek² | Ming Zhang¹ 

¹School of Materials Science and Engineering, Zhejiang Sci-Tech University, Hangzhou, China

²Institute for Nanomaterials, Advanced Technologies and Innovations, Technical University of Liberec, Liberec, Czech Republic

Correspondence

Ming Zhang, School of Materials Science and Engineering, Zhejiang Sci-Tech University, Hangzhou 310018, China.
Email: zhangming@zstu.edu.cn

Funding information

International Science and Technology Cooperation Programme (CN), Grant/Award Number: 2016YFE0131400

Abstract

Recent years, phase change materials (PCMs) with potential to store and transform energy have attracted broad attention, especially in the field of thermal energy storage. However, the instability and leak proneness of PCMs limit their universal application. In this paper, core-shell fibers with 1-tetradecanol (TD) as core and poly(vinylidene fluoride) (PVDF) as shell were prepared via melt coaxial electrospinning method, and for improvement, the dye composed of crystal violet lactone (CVL) and bisphenol A (BPA) was added to the core to endow the fiber the function of reversible thermochromism. During the preparation process, it was found that the addition of NaCl could regulate the fiber morphology and strength its mechanical property. By adjusting the concentration of shell solution and the flow rate of core solution, the high-strength reversible thermochromic fibers were produced when polymer concentration was 24 wt% with a core feed rate of 0.4 ml/h. The latent heat of these fibers is up to 88.71 J/g. Besides, its color can change from blue to white when heated, and the transition temperature is around 38°C. And 100 thermal cycle tests of the fiber showed its strong thermal stability and thermochromic property.

KEYWORDS

electrospinning, fibers, nanostructured polymers, textiles

1 | INTRODUCTION

The storage of fossil energy continues to decrease, and what is more serious is that its extensive use causes pollution to the environment,^{1–3} prompting people to study clean and renewable energy. Thermal energy storage is currently one of the most efficient energy storage methods, shows great promise as a means of environmental protection and energy reduction. Phase change materials (PCMs) can absorb, store, or release a large amount of latent heat at a constant temperature,^{4,5} so they play important roles in different application fields, such as, temperature regulation, energy-saving, buildings, and smart fabrics.^{6–8}

PCMs are commonly divided into inorganic and organic compounds based on their chemical constituents,^{9,10} which can maintain stable thermal properties after multiple phase change cycles. At present, organic PCMs are most used and studied because they have the advantages of negligible corrosion and super-cooling degree compared with inorganic PCMs.¹¹ According to the type of phase change, PCMs include four species: solid–solid, solid–liquid, solid–gas, and liquid–gas. Solid–liquid PCMs have remarkable superiority over the other PCMs in terms of small volume change during the phase change process, high latent heat storage, and low cost,¹² indicating that they have great practical applicability. A typical organic solid–liquid PCM, 1-tetradecanol (TD), exhibiting remarkable properties, such as, high latent

heat, non-toxic, non-corrosive, and good thermal stability.^{13,14} Moreover, the phase transition temperature of TD is close to the human body temperature, which is very suitable for the application of smart textiles. Nevertheless, like other solid-liquid PCMs, TD will inevitably leak into the surrounding environment during the repeated cycles of melting and cooling, which shorten its usable life.¹⁵⁻¹⁷

At present, commonly used methods include sol-gel, microencapsulation, and electrospinning to produce shape-stable composite PCMs.¹⁸⁻²⁰ These methods can fix the PCM on the solid substrate and effectively prevent its leakage. It is troublesome to use products prepared by sol-gel and microencapsulation in textiles. Electrospinning is different. It is a one-step technique for adding PCMs to electrospun fibers and can be directly applied to textile field.^{21,22} In particular, coaxial electrospinning, which uses a polymer shell to encapsulate PCM in the core of the fibers to prepare nanofibers with core-shell structure, has received increasing attention.²³⁻²⁵ The smart nanofibers with core-shell structures have attractive advantages of ultra-fine size, high specific surface area, and stable thermal performance.^{26,27} Therefore, they could apply in thermal regulation of clothing and electronic components. Currently, solution coaxial electrospinning is the most used method due to its simple equipment and convenient operation,²⁸ but the latent heat of the prepared fiber is generally low. For example, Yu et al. chose soy wax as core material and polyurethane as shell material, and its latent heat was 36.47 J/g.²⁹ Lu et al. fabricated encapsulated paraffin wax nanofibers, and the latent heat was 58.25 J/g.³⁰ Compared with solution coaxial electrospinning, melt coaxial electrospinning is characterized by no solvent in the core, so the packaging efficiency of PCM is greatly improved.³¹

With the rapid development of energy storage materials, the single function of thermal storage can no longer meet people's needs. Adding some functional materials into the fibers can respond to external stimuli, such as, light, heat, electric, and magnetic fields, making these materials have applications in monitoring, control, and sensing.³²⁻³⁵ Phase change thermochromic materials have received widespread attention due to their heat-sensitive reversible color and temperature regulation characteristics. The Japanese Dream Company has produced color-changing octopus toys, which are deeply loved by children. Thermochromic nanofibers perform high sensitivity and temperature responsiveness for use in medical, safety, and quality control fields. Ilana Malherbe et al. have prepared reversible thermochromic microfibers by solution coaxial electrospinning, while they did not measure the specific enthalpy of the fiber and the low temperature of discoloration is not practical.³⁶ Thermochromic materials used in fabric field usually consist of leuco dyes, developers, and phase-change

medium. The most commonly used and studied leuco dye is crystal violet lactone, which most significant characteristic is the obvious chromaticity change. Color developers are weak acids, which act as proton donors to initiate the color development of leuco dye. The phase change medium also acts as a solvent for dyes and developers, and it can be fatty alcohol or ester. The color transition temperature of these thermochromic fibers is determined by the melting temperature of the solvent, so the color change temperature can be regulated by replacing the PCMs.³⁷

Herein, we present a study of reversibly thermochromic core-shell nanofibers using melt coaxial electrospinning. Poly(vinylidene fluoride) (PVDF) is used as the polymer shell, which has good thermal stability, high mechanical strength, and light transmittance. The thermochromic composite has consisted of CVL as a dye, BPA as a developer, and TD as a phase-change medium. Adding NaCl to the shell solution could enhance the conductivity and improve the morphology and mechanical strength of the fibers.³⁸⁻⁴⁰ We also systematically discussed the influence of shell solution concentration and core feed rate on the encapsulation rate. The result stated that the final latent heat of the thermochromic fiber could be as high as 88.71 J/g. Consecutive 100 recycle phase change experiments were conducted to prove the optimized sample has good reusability. The functional fiber developed through this work exhibits excellent latent heat and reversible thermochromic properties, so it has broad application prospects in body-temperature thermal materials and thermoresponsive sensors. Moreover, the fiber has high strength, providing huge potential applications in thermal protective clothing.

2 | EXPERIMENTAL

2.1 | Materials

Poly(vinylidene fluoride) (PVDF, $M_w = 4 \times 10^5$), bisphenol A (BPA, CP, $M_w = 288.96$), 1-tetradecanol (AR, 96%) and N,N-dimethyl acetamide (DMAc) were purchased from Aladdin Chemistry Co., Ltd. Crystal violet lactone (CVL, $M_w = 415.53$) was purchased from Beijing Bailingwei Technology Co., Ltd. Ethanol and NaCl was purchased from Hangzhou Gaojing Fine Chemical Industry Co., Ltd.

2.2 | Preparation of core-shell nanofiber membrane

To obtain the shell solution, PVDF with different concentrations of 22, 24, and 26 wt % was added into DMAc with magnetic stirring at 55°C for 12 h. NaCl with

concentration of 0.02 wt % was added into the shell solutions, and the other conditions were as above. Before spinning, TD needs to be heated at 90°C for 2 h to melt. The thermochromic composite was to mix CVL, BPA, and TD (CBT, CBT stands for a mixture of CVL, BPA, and TD) at a weight ratio of 1: 5: 115, and magnetically stir at 90°C for 2 h to obtain a uniform solution. The stainless-steel coaxial needle was composed of an inner needle and an outer needle. The inner and outer diameters of the inner needle were 0.41/0.72 mm, and the inner and outer diameters of the outer needle were 1.01/1.49 mm. The applied voltage was 28 kV, and the distance between nozzle and collector was about 20 cm. The shell solution feed rate was 1.5 ml/h, and the core solution feed rate was adjusted to 0.3, 0.4, and 0.5 ml/h, respectively. The spinning ambient temperature was controlled at 55°C and the relative humidity was 50%.

2.3 | Thermal cycle test

In order to study the thermal stability of the prepared fibers, melt-cooling cycles were conducted in a thermostatic oven between 25 and 50°C. These film samples were firstly heated above the melting temperature (38°C) and then cooled to the room temperature (25°C), which is one thermal periodical cycle. After 100-thermal cycles, the enthalpy of samples was measured by differential scanning calorimetry (DSC, Q2000) to study their thermal stability.

2.4 | Characterizations

The morphology of PVDF@TD and PVDF-NaCl@TD (PVDF@TD means core-shell structured, with PVDF shell and TD core fibers, NaCl means adding NaCl to PVDF solution) was obtained by the field emission scanning electron microscopy (FE-SEM, ULTRA55, Zeiss) at an acceleration voltage of 3 kV. Before observation, the samples need to be soaked in ethanol for 24 h to remove the inner liquor and then coated with thin layers of gold. The diameters of 30 random fibers were measured by ImageJ software, and then their average diameters were calculated to represent the diameter of fibers prepared under different conditions. The PVDF-NaCl@CBT- $V_{0.4}$ ($V_{0.4}$ means that the core feed rate is 0.4 ml/h) core-shell structure of the nanofibers was studied by the transmission electron microscope (TEM, JEM-2100, JOEL) at an acceleration voltage of 200 kV. The TEM samples were prepared by depositing nanofibers on a 400-mesh carbon-coated Cu grid and then immersing it in ethanol for 24 h. Thermal stability and decomposition properties of the

specimens were obtained by thermogravimetric analysis (L81/1750TGA, LINSEIS Company, Germany). Fourier transform infrared spectroscopy (FTIR) of the nanofibers was conducted on a Nicolet 5700 FTIR spectrometer from 4000 to 350 cm^{-1} in the transmittance mode. DSC tests were implemented in nitrogen flow, and the samples were heated from 0 to 50°C and then cooled from 50 to 0°C, the heating and cooling rate were 10 K/min. The latent heat of the fibers is directly analyzed by TRIOS software. The tensile performance of fibers was conducted in the STD standard tensile method. All samples for mechanical testing were cut into small pieces of 0.5×2 cm, and the thickness of each sample was measured separately.

3 | RESULTS AND DISCUSSION

The typical coaxial electrospinning technique was applied to fabricate reversible thermochromic core-shell nanofibers. As shown in Figure 1, the coaxially arranged needles linking with two separate syringes containing different solutions through plastic tubes: connect the shell solution to the outer, and the core solution to the inner. Applying a suitable high voltage between the needle and the collector, where the electric field force stretches the solution to form jet, so that the fibers can be obtained from the collector. The method fixes the PCMs in the center of the nanofibers, and the polymeric shell can maintain the stability of the fiber shape, which can effectively prevent the leakage of the PCMs.

Figure 2 shows the morphology of PVDF@TD with different polymer concentrations, at the core feed rate of 0.3 ml/h. The fibers are messy with a lot of beads and scarcely in long straight, which was attributed to the poor conductivity and high surface tension of the shell solution resulting in the insufficient electric field force to stretch the polymer. Adding NaCl to the shell solution to enhance the conductivity, the increase of the electric field force will stimulate the stretching effect, and strengthen the whiplash effect of the solution jet during the electrospinning process, which can make the fibers more uniform.^{38,40,41} Figure 3 is the morphology of PVDF-NaCl@TD with different PVDF concentrations and core feed rates. When PVDF concentration is 22 wt% (Figure 3 (a)-(c)), fibers still have much bead-like structure, but it has been improved compared with before. And when PVDF concentration increased to 24 (Figure 3(d)-(f)) and 26 (Figure 3(g)-(i)) wt%, the fibers became straight and cylindrical, with a basically bead-free structure. The cause of these two different morphologies is polymer concentration. The solution with low concentration has a high surface tension that tends to transform the jet into

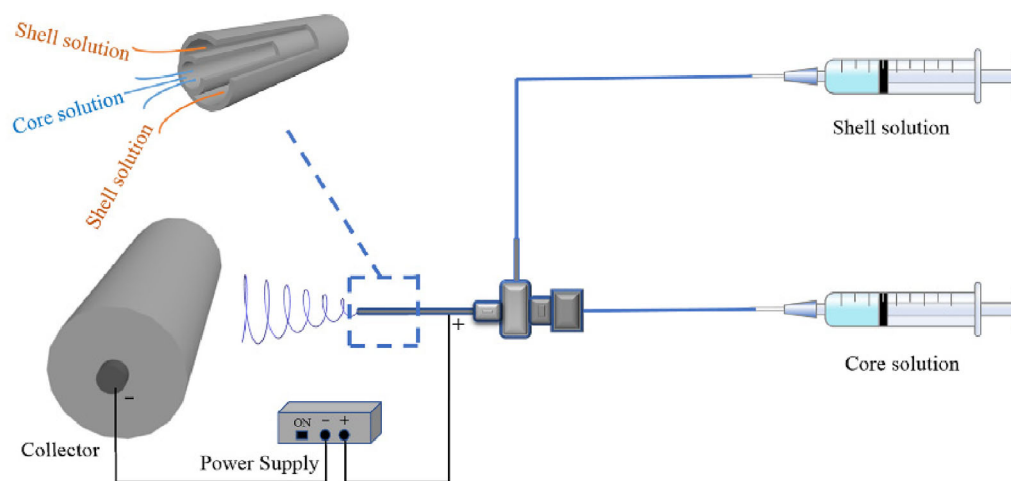


FIGURE 1 Schematic illustration of the coaxial electrospinning technique [Color figure can be viewed at wileyonlinelibrary.com]

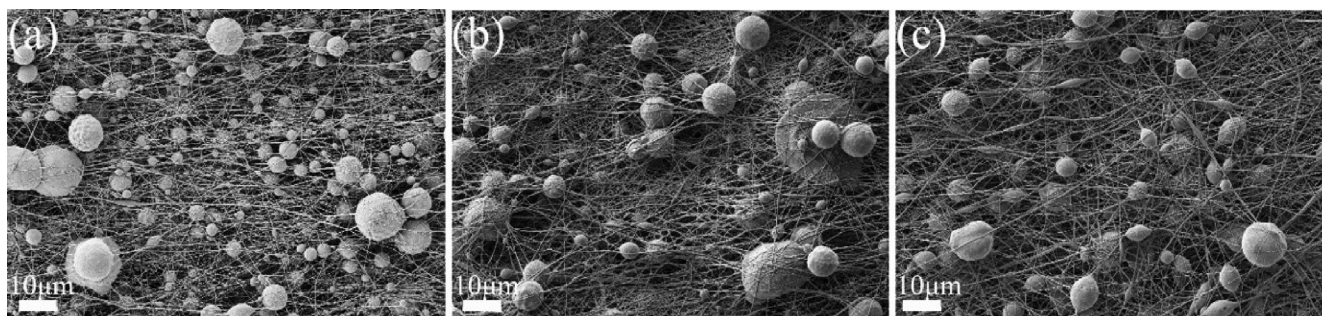


FIGURE 2 The FE-SEM images of the PVDF@TD with core feed rate of 0.3 ml/h and PVDF concentrations (wt%) of (a) 22%; (b) 24%; and (c) 26%

spherical droplets forming bead-like fibers.^{42–44} Therefore, appropriate solution concentration is also crucial in the electrospinning process.

Figure 4 shows the average diameter of PVDF-NaCl@TD with different PVDF solution concentrations and core feed rates. It clearly shows that keeping the concentration of the shell solution constant, the diameter of the fiber increases with the increase of the core feed rate. Because as the core feed speed increases, more core material can be encapsulated, making the fiber diameter larger. Besides, the same trend can also be found under different concentrations of the PVDF solution. The augment of the solution concentration strengthens the molecular chain entanglement, which makes the solution viscosity increase. Therefore, the splitting performance of the droplets decreases, which causes the fibers to become bolder.

The DSC thermograms of PVDF-NaCl@TD are shown in Figure 5, with the corresponding summarized data listed in Table 1. For pure PVDF, no phase change occurs (as shown in Figure S1). There are two obvious exothermic peaks during the crystallization process,

which are due to the existence of a metastable intermediate solid phase. However, in the melting process, because the temperature of the solid-metastable solid and metastable solid-liquid transition is very close and indistinguishable, there is only one peak.¹³ It can be found that when the shell concentration is constant, as the core feed rate increases, the latent heat deceleration of the fiber augments and finally reaches the peak value, which means the maximum encapsulation rate under this condition. For example, at the concentration of 26 wt%, the variation of latent heat is inconsistent with the core feed rate. Because when the core feed rate is low, the polymer can encapsulate the PCMs well. However, as the core feed rate increases, the viscosity of the polymer solution is not enough to drag the core solution, resulting in redundant PCMs that will inevitably leak. Therefore, the improvement in latent heat slows down and tends to stabilize.⁴⁵ It's the same at other concentrations. The highest latent heat obtained is 148.26 J/g, but the morphology of the fibers is bead-like. Besides, when the core feed rate is constant, the latent heat decreases as the concentration of the PVDF solution increases. Because the increase in

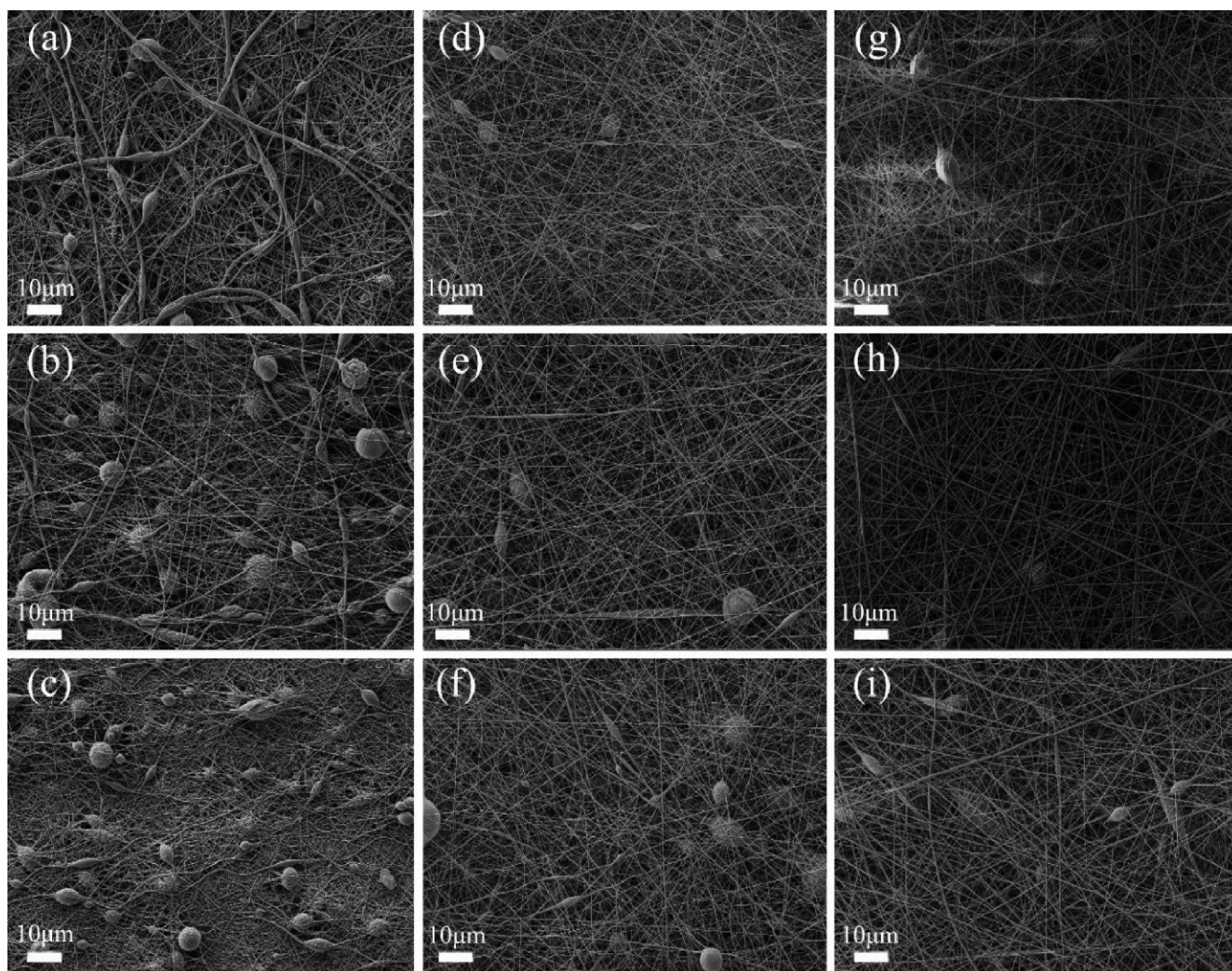


FIGURE 3 The FE-SEM images of the PVDF-NaCl@TD with different PVDF concentrations (wt%): (a-c) 22%; (d-f) 24%; (g-i) 26%; samples with different core feed rates: (a, d, and g) 0.3 ml/h; (b, e, and h) 0.4 ml/h; (c, f, and i) 0.5 ml/h

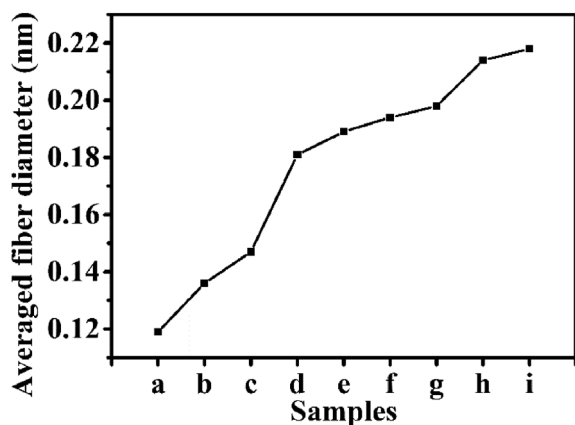


FIGURE 4 Diameter distributions of the PVDF-NaCl@TD prepared under different conditions

the concentration of the PVDF solution only improves the composition of PVDF in the core-shell structure fibers, while PVDF only contributes to the increase in

weight without phase change, so the latent heat decreases.⁴⁵ Finally, considering the morphology and latent heat, the optimal preparation conditions were determined as the shell solution concentration of 24 wt% and the core feed rate of 0.5 ml/h.

To further functionalize the fibers, CVL, and BPA were added to prepare reversible thermochromic fibers. As expected, PVDF encapsulated CBT formed an ideal core-shell structure, as demonstrated in Figure 6. The digital pictures of PVDF-NaCl@CBT membranes are shown in Figure 7. Before adding the dye, the as-prepared membrane is white, and that in Figure 7(a) is blue, which also indicates that the polymer successfully encapsulated the dye. However, there are many blue spots on the surface of the membrane, which may be excess core solution droplets that are not encapsulated by the shell due to the core feed rate being too fast. Therefore, the core feed rate should be adjusted to 0.4 ml/h, and the resulting membrane shown in Figure 7(b). After

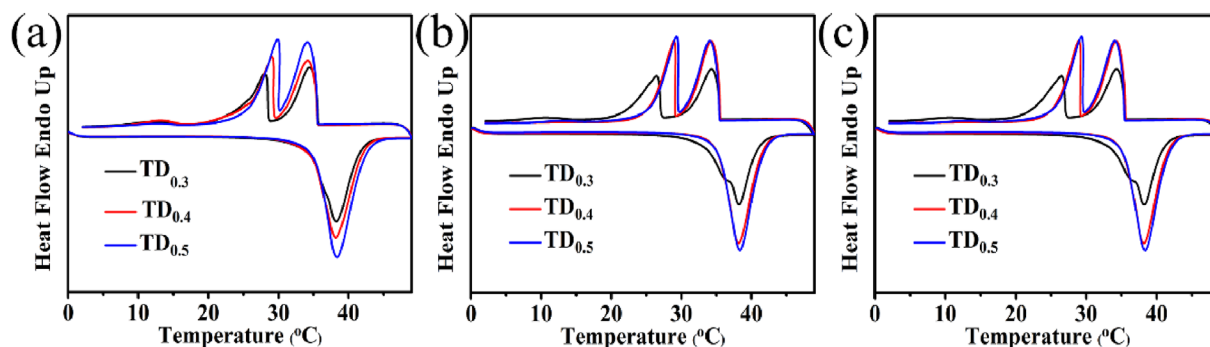


FIGURE 5 The differential scanning calorimetry curves of PVDF-NaCl@TD with different core feed rates and PVDF concentrations (wt %): (a) 22%; (b) 24%; and (c) 26% [Color figure can be viewed at wileyonlinelibrary.com]

TABLE 1 The differential scanning calorimetry analyses data of PVDF-NaCl@TD with different PVDF concentrations and core feed rates

Concentration (wt%)	Feed rate (ml/h)	T_m (°C)	ΔH_m (J/g)	T_t (°C)	T_c (°C)	ΔH_{t+c} (J/g)
22%	0.3	38.24	107.20	28.01	34.46	97.22
	0.4	38.17	129.90	29.08	34.20	112.16
	0.5	38.36	146.26	29.89	34.19	138.00
24%	0.3	38.22	73.92	26.64	34.32	66.16
	0.4	38.16	98.06	28.94	34.25	95.85
	0.5	38.35	108.59	29.31	34.08	102.67
26%	0.3	37.74	71.50	27.16	33.97	65.45
	0.4	38.16	90.58	28.30	34.13	82.56
	0.5	38.13	91.60	28.56	34.11	82.28

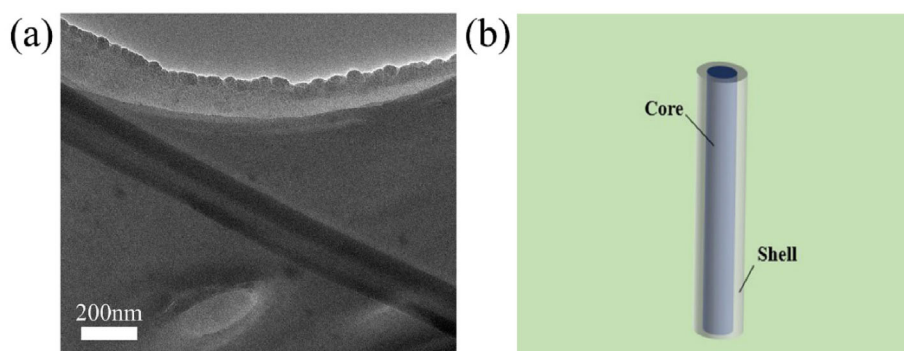


FIGURE 6 (a) The transmission electron microscope image of PVDF-NaCl@CBT- $V_{0.4}$; (b) the core-shell structure model [Color figure can be viewed at wileyonlinelibrary.com]

reducing the core material feed rate, the morphology of the membrane was optimized to make it spotless and uniform in color. The color state of the fibers decides by the reaction of the electron donor and electron acceptor. When the temperature is lower than the melting temperature of TD, BPA releases protons and gain electrons, forming a complex with CVL that favors the colored ring-open, where molecular rearrange and conjugate double bond through, which show the color. As the temperature rises above the melting temperature of TD, the color developer combined with protons, and the leuco dye favors the colorless, ring-closed

state.⁴⁶ Therefore, the PVDF-NaCl@CBT- $V_{0.4}$ membrane can repeatedly show color and colorless (Figure 7(c)) state according to temperature changes.

Figure 8 and Table 2 show the performance of PVDF-NaCl@CBT- $V_{0.4}$ before and after 100 thermal cycles. The latent heat of these fibers is 88.071 J/g, which is better than some functional fibers.^{33,47} After thermal cycling treatment, the T_m and ΔH_m decreased by 1.79°C and 2.06 J/g, respectively, without significant changes. Through the comparison of fiber properties before and after thermal cycling, it can be concluded that PVDF-NaCl@CBT- $V_{0.4}$ possesses

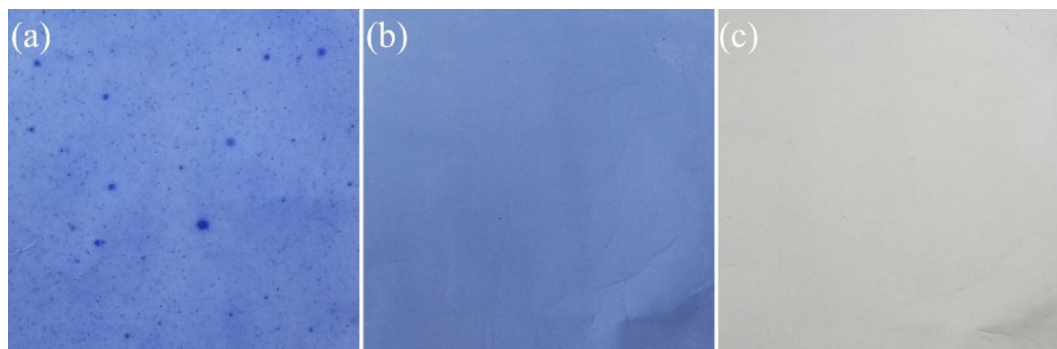
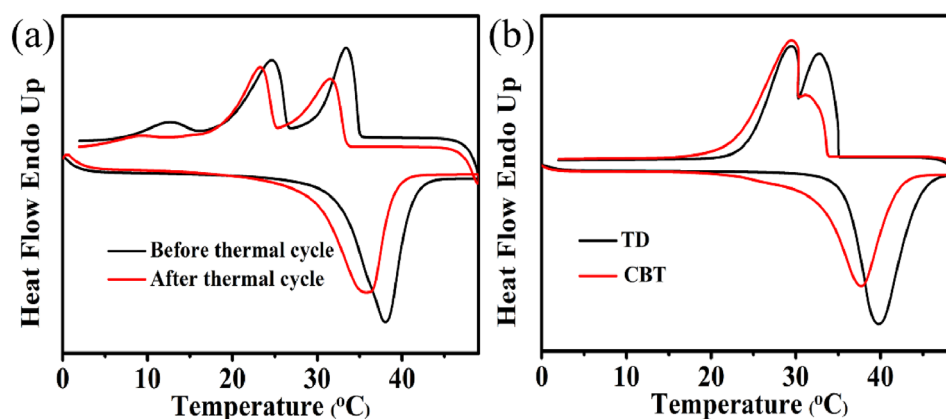


FIGURE 7 Images of PVDF-NaCl@CBT membrane with core feed rate of (a) 0.5 ml/h at 15°C; (b) 0.4 ml/h at 15°C; (c) 0.4 ml/h at 45°C [Color figure can be viewed at wileyonlinelibrary.com]

FIGURE 8 The differential scanning calorimetry curves of (a) PVDF-NaCl@CBT- $V_{0.4}$ before and after 100 cycles; (b) TD; and CBT [Color figure can be viewed at wileyonlinelibrary.com]



excellent thermal stability and reliability. Besides, combining the DSC data of TD and CBT found that the reduction of the latent heat of the fiber is inevitable after adding the dye. This might be attributed to two factors: (a) the added dye only increases the weight without phase transition occurs, which leads to a decrease in enthalpy, and (b) some aggregation and hindrance to TD from the dye play a dominant effect, which is attributed to molecular limitations.⁴⁸

Thermogravimetric analysis (TGA) was used to evaluate the thermal stability of PVDF, CBT, and PVDF-NaCl@CBT- $V_{0.4}$. The results are shown in Figure 9 in terms of the percentage of weight loss versus temperature. The experimental results show that CBT completely decomposed at about 260°C, and PVDF began its degradation at 460°C. On the other hand, PVDF-NaCl@CBT- $V_{0.4}$ showed two degradation stages. For the composite fibers, the first stage corresponds to the decomposition of CBT molecules, and the second stage is the decomposition of PVDF matrices. It can be seen from the figure that the decomposition rate of CBT decreases, indicating that the encapsulation of PVDF improves its thermal stability.^{12,31} It shows that the core-shell structure fiber can increase its decomposition temperature, which is very important in practical applications. Figure 10 represented the Fourier transform infrared spectroscopy (FTIR) spectra of PVDF,

CBT, and PVDF-NaCl@CBT- $V_{0.4}$. The absorption peaks of PVDF at 1754 and 1402 cm^{-1} correspond to the bending vibration and tensile vibration of C—F₂. Besides, the peak at 840 cm^{-1} belongs to the C—F stretch band.⁴⁹ From the CBT spectrum, several absorption peaks can be observed, in which the peaks at 2956, 2920, and 2850 cm^{-1} belonged to the symmetrical stretching vibration of its —CH₃ and —CH₂ group.^{50,51} Meanwhile, the absorption peaks at 1471 and 717 cm^{-1} represent the bending vibration of the —CH₂ group and the in-plane swing vibration of the —OH group.⁵¹ The spectra of composite fibers show all the characteristic bands of the two components with no new peak formed, implying that PVDF and CBT did not interact in any way. It was further confirmed that PVDF successfully encapsulated CBT.

The stress-strain curves are presented in Figure 11. The mechanical strength of the pure PVDF nanofiber membrane with a concentration of 24 wt% is low because fibers have many unevenly distributed beads that make them unable to withstand large external forces.³⁸ With the addition of NaCl, the enhanced conductivity of the solution facilitates the orientation and aggregation of macromolecules in the fibers, which greatly improves the mechanical properties of the fibers.^{40,41} When PVDF encapsulates CBT, the mechanical strength of the fibers

Samples	T_m (°C)	ΔH_m (J/g)	T_t (°C)	T_c (°C)	ΔH_{t+c} (J/g)
TD	39.76	274.15	29.44	35.24	272.36
CBT	37.71	238.25	29.26	34.17	230.53
Before thermal cycle	38.04	88.71	24.65	34.43	85.27
After thermal cycle	36.25	86.65	23.31	33.49	82.48

TABLE 2 The differential scanning calorimetry analysis of PVDF-NaCl@CBT-V_{0.4} before and after thermal cycle, TD, and CBT

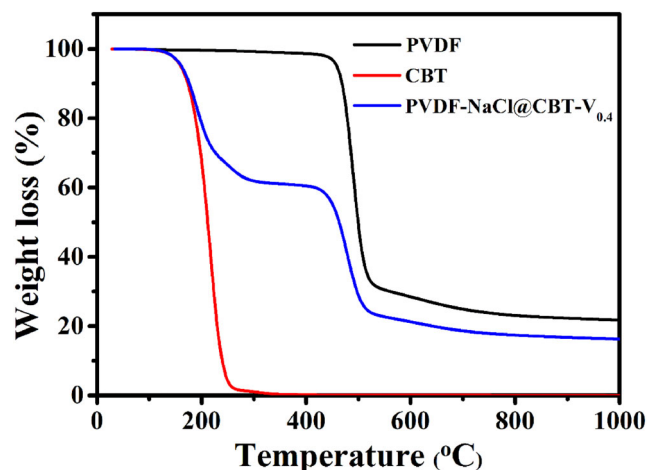


FIGURE 9 Thermogravimetric analysis curves of PVDF, CBT, and PVDF-NaCl@CBT-V_{0.4} [Color figure can be viewed at wileyonlinelibrary.com]

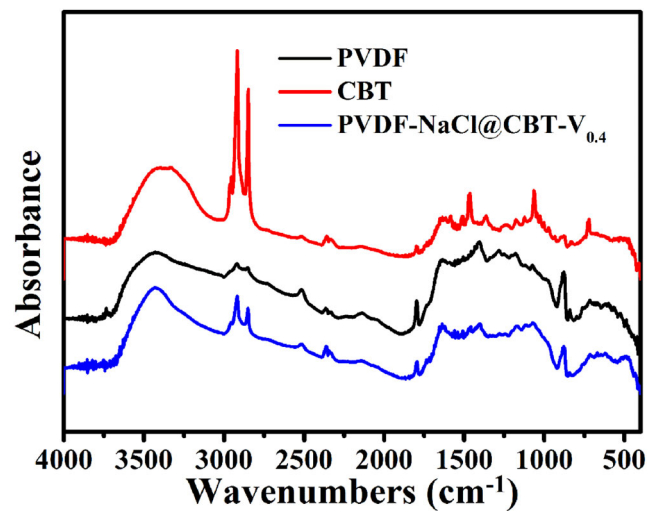


FIGURE 10 Fourier transform infrared spectra of PVDF, CBT, and PVDF-NaCl@CBT-V_{0.4} [Color figure can be viewed at wileyonlinelibrary.com]

decreases because of the load of brittle 1-tetradecanol.⁴⁵ Compared to some core-shell fibers previously reported,^{12,31,52} PVDF-NaCl@CBT-V_{0.4} has excellent mechanical properties, indicating that it has a good application prospect in the production of protective clothing.

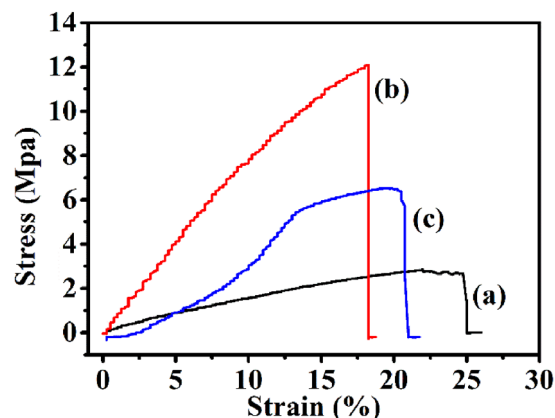


FIGURE 11 Stress-strain curves of nonwoven mats of (a) PVDF nanofibers; (b) PVDF with 0.02 wt% NaCl nanofibers; and (c) PVDF-NaCl@CBT-V_{0.4} [Color figure can be viewed at wileyonlinelibrary.com]

4 | CONCLUSIONS

In summary, reversible thermochromic core-shell nanofibers were successfully prepared by encapsulating CBT using PVDF through melt coaxial electrospinning technique. The addition of NaCl improves the morphology and mechanical properties of the fibers. By adjusting the shell solution concentration and core feed rate, the optimal PVDF-NaCl@CBT-V_{0.4} possesses obvious reversible thermochromic performance and high latent heat up to 88.71 J/g. The encapsulation and fixing of thermochromic composite actualize their potential applications in thermal protective clothing and thermo-responsive sensors. Moreover, 100 thermal cycle tests show that the nanofibers have good thermal stability and thermochromic properties, indicating that the PCMs leakage problem is well overcome. Hence, this work provides a strong support for the research and development of functional fibers.

ACKNOWLEDGMENTS

The authors acknowledge financial support from Key Program for International Cooperation Projects of China (2016YFE0131400).

CONFLICT OF INTEREST

The authors declare no potential conflict of interest.

ORCID

Ming Zhang  <https://orcid.org/0000-0002-2916-8128>

REFERENCES

- [1] B. Rezaei, M. Ghani, M. Askari, A. M. Shoushtari, R. M. A. Malek, *Adv. Polym. Technol.* **2016**, *35*, 21534.
- [2] D. Yang, S. Shi, L. Xiong, H. Guo, H. Zhang, X. Chen, C. Wang, X. Chen, *Sol. Energy Mater. Sol. Cells* **2016**, *144*, 228.
- [3] C. Chen, L. Wang, Y. Huang, *Mater. Lett.* **2008**, *62*, 3515.
- [4] W. Chalco-Sandoval, M. J. Fabra, A. López-Rubio, J. M. Lagaron, *Eur. Polym. J.* **2015**, *72*, 23.
- [5] R. Semnani Rahbar, H. Maleki, B. Kalantari, *J. Exp. Nanosci.* **2016**, *11*, 1402.
- [6] S.-X. Sun, R. Xie, X.-X. Wang, G.-Q. Wen, Z. Liu, W. Wang, X.-J. Ju, L.-Y. Chu, *J. Mater. Sci.* **2015**, *50*, 5729.
- [7] E. C. B. Noyan, E. Onder, N. Sarier, R. Arat, *Thermochim. Acta* **2018**, *662*, 135.
- [8] M. K. Rathod, J. Banerjee, *Renewable Sustainable Energy Rev.* **2013**, *18*, 246.
- [9] Y. Wu, C. Chen, Y. Jia, J. Wu, Y. Huang, L. Wang, *Appl. Energy* **2018**, *210*, 167.
- [10] W. Hu, X. Yu, *Renewable Energy* **2014**, *62*, 454.
- [11] S. C. Lin, H. H. Al-Kayiem, *Appl. Mech. Mater.* **2014**, *699*, 263.
- [12] C. V. Do, T. T. T. Nguyen, J. S. Park, *Korean J. Chem. Eng.* **2013**, *30*, 1403.
- [13] H. Yang, S. Wang, X. Wang, W. Chao, N. Wang, X. Ding, F. Liu, Q. Yu, T. Yang, Z. Yang, J. Li, C. Wang, G. Li, *Appl. Energy* **2020**, *261*, 114481.
- [14] H. Wang, P. Gui, Y. Zhu, S. Hu, *J. Wuhan Univ. Technol. Mater. Sci. Ed.* **2020**, *35*, 327.
- [15] Y. Lu, X. Xiao, J. Fu, C. Huan, S. Qi, Y. Zhan, Y. Zhu, G. Xu, *Chem. Eng. J.* **2019**, *355*, 532.
- [16] Y. Wan, P. Zhou, Y. Liu, H. Chen, *RSC Adv.* **2016**, *6*, 21204.
- [17] C. Chen, L. Wang, Y. Huang, *Polymer* **2007**, *48*, 5202.
- [18] H. Ke, Q. Wei, *Thermochim. Acta* **2019**, *671*, 10.
- [19] A. Sari, C. Alkan, A. Karaipekli, *Appl. Energy* **2010**, *87*, 1529.
- [20] A. Babapoor, G. Karimi, M. Khorram, *Appl. Therm. Eng.* **2016**, *99*, 1225.
- [21] F. Haghghat, S. A. Hosseini Ravandi, M. Nasr Esfahany, A. Valipouri, *J. Mater. Sci.* **2017**, *53*, 4665.
- [22] F. E. Ahmed, B. S. Lalia, R. Hashaikeh, *Desalination* **2015**, *356*, 15.
- [23] G. Duan, A. Greiner, *Macromol. Mater. Eng.* **2019**, *304*, 1800669.
- [24] H. F. Alharbi, M. Luqman, H. Fouad, K. A. Khalil, N. H. Alharthi, *Polym. Test.* **2018**, *67*, 136.
- [25] F. Nasiri, S. Ajeli, D. Semnani, M. Jahanshahi, H. Morad, *J. Textiles Polym.* **2020**, *8*, 1.
- [26] A. Babapoor, G. Karimi, S. I. Golestaneh, M. A. Mezjin, *Appl. Therm. Eng.* **2017**, *118*, 398.
- [27] X. Zhang, R. Xie, W.-X. Hu, Y. Faraj, Q. Zhao, X.-X. Fan, W. Wang, X.-J. Ju, Z. Liu, L.-Y. Chu, *J. Mater. Sci.* **2018**, *53*, 15769.
- [28] Y. Lu, X. Xiao, J. Mo, C. Huan, S. Qi, Y. Zhan, Y. Zhu, G. Xu, *Colloids Surf., A* **2018**, *555*, 501.
- [29] W. Hu, X. Yu, *RSC Adv.* **2012**, *2*, 5580.
- [30] Y. Lu, X. Xiao, Y. Zhan, C. Huan, S. Qi, H. Cheng, G. Xu, *ACS Appl. Mater. Interfaces* **2018**, *10*, 12759.
- [31] C. Van Do, T. T. T. Nguyen, J. S. Park, *Sol. Energy Mater. Sol. Cells* **2012**, *104*, 131.
- [32] O. Mapazi, K. P. Matabola, R. M. Moutloali, C. J. Ngila, *Polymer* **2018**, *149*, 106.
- [33] Y. Lu, X. Xiao, Y. Liu, J. Wang, S. Qi, C. Huan, H. Liu, Y. Zhu, G. Xu, *J. Alloys Compd.* **2020**, *812*, 152144.
- [34] J. Nguyen, R. M. Stwodah, C. L. Vasey, B. E. Rabatin, B. Atherton, P. A. D'Angelo, K. W. Swana, C. Tang, *Polymer*, **2020**, *12*, 842.
- [35] Z. Qin, P. Zhang, Z. Wu, M. Yin, Y. Geng, K. Pan, *Mater. Des.* **2018**, *147*, 175.
- [36] I. Malherbe, R. D. Sanderson, E. Smit, *Polymer* **2010**, *51*, 5037.
- [37] F. Li, Y. Zhao, S. Wang, D. Han, L. Jiang, Y. Song, *J. Appl. Polym. Sci.* **2009**, *112*, 269.
- [38] J. Gu, H. Gu, J. Cao, S. Chen, N. Li, J. Xiong, *Appl. Surf. Sci.* **2018**, *439*, 589.
- [39] J. Zhao, W. Zhu, W. Yan, X. Wang, L. Liu, J. Yu, B. Ding, *Compos. Commun.* **2019**, *15*, 40.
- [40] L. Zhang, Y. Li, J. Yu, B. Ding, *RSC Adv.* **2015**, *5*, 79807.
- [41] D. Poudel, S. Swilley-Sanchez, S. O'Keefe, J. Matson, T. Long, C. Fernandez-Fraguas, *Polymer*, **2020**, *12*, 2558.
- [42] J. M. Deitzel, J. Kleinmeyer, D. Harris, N. C. Beck Tan, *Polymer* **2001**, *42*, 261.
- [43] Y. P. Neo, S. Ray, A. J. Easteal, M. G. Nikolaidis, S. Y. Quek, *J. Food Eng.* **2012**, *109*, 645.
- [44] J. Doshi, D. H. Reneker, *J. Electrostatic* **1995**, *35*, 151.
- [45] L. Yi, Y. Wang, Y. Fang, M. Zhang, J. Yao, L. Wang, J. Marek, *RSC Adv.* **2019**, *9*, 21844.
- [46] X. Geng, W. Li, Y. Wang, J. Lu, J. Wang, N. Wang, J. Li, X. Zhang, *Appl. Energy* **2018**, *217*, 281.
- [47] Y. He, S. Sun, N. Han, X. Zhang, W. Li, *J. Mater. Sci.* **2020**, *55*, 12921.
- [48] S. Li, H. Wang, H. Mao, J. Li, H. Shi, *ACS Appl. Mater. Interfaces* **2019**, *11*, 14150.
- [49] Y. Cui, T. Zhang, Y. Feng, C. Zhang, Q. Chi, Y. Zhang, Q. Chen, X. Wang, Q. Lei, *Composites, Part B* **2019**, *177*, 107429.
- [50] S. Özkayalar, E. Adigüzel, S. Alay Aksoy, C. Alkan, *Mater. Chem. Phys.* **2020**, *252*, 123162.
- [51] C. Wang, Z. Hu, Q. A. Yin, X. Liu, Q. Liu, C. Bao, *J. Polym. Res.*, **2020**, *27*.
- [52] E. Zdraveva, J. Fang, B. Mijovic, T. Lin, *Ind. Eng. Chem. Res.* **2015**, *54*, 8706.

SUPPORTING INFORMATION

Additional supporting information may be found online in the Supporting Information section at the end of this article.

How to cite this article: Wang S, Yi L, Fang Y, et al. Reversibly thermochromic and high strength core-shell nanofibers fabricated by melt coaxial electrospinning. *J Appl Polym Sci.* 2021;138:e50465. <https://doi.org/10.1002/app.50465>